（平成１７年度）

書籍

著者氏名	論文タイトル名	書籍全体の編集者名	書　籍　名	出版社名	出版地	出版年	ページ
佐粧久、守屋秀繁	変形性膝関節症	守屋秀繁	整形外科　診療実践ガイド	分光堂	東京	2006	844-846

雑誌

発表者氏名	論文タイトル名	発表誌名	巻号	ページ	出版年
Matsuyama J, Ohnishi I, Sakai R,Suzuki H, Harada A, Besshi M, Masumoto T, Nakamura K	A new method for measurement of bone deformation by echo tracking.	Med Eng Phys	26		2005
Ohashi S, Ohnishi I, Kageyama T, Fukuda S, Tsuchiya A, Imai K, Matsuyama J, Nakmura K	Effect of vascularity on canine distracted tibial callus consolidation.	Clin Orthop Relat Res	438	253-259	2005
Matsuyama J, Ohnishi I,Kageyama T, Oshida H, Suwabe T, Nakamura K	Osteogenesis and angiogenesis in regenerating bone during transverse distraction:quantitative evaluation using a canine model,	Clin Orthop Relat Res	433	243-250	2005
Matsudaira K, Yamazaki T, Seichi A, Takeshita K, Hoshi K, Kishimoto J, Nakamura K	Spinal stenosis in grade 1 degenerative lumbar spondylolisthesis: a comparative study of outcomes following laminoplasty and laminectomy with instrumented spinal fusion.	J Orthop Sci	10	270-276	2005
Ohnishi I, Kurokawa T, Sato W, Nakamura K	Measurement of the tensile forces during bone lengthening.	Clin Biomech	20	421-427	2005
Ohnishi I, Sato W, Matsuyama J, Yajima H, Haga N, Kamegaya M, Minami A, Sato M, Yoshino S, Oki T, Nakamura K	Treatment of congenital pseudarthrosis of the tibia: A multicenter study in Japan.	J Pediatr Orthop	25	219-224	2005

Fujiwara S, Nakamura I, Higo R, Tajiri Y, Nakamura K, Oda H	A case report of repeated postoperative laryngeal obstruction due to bilateral cricoarytenoid joint involvement in rheumatoid arthritis.	Mod Rheumatol	15	123-125	2005
Hikita A, Kdomo Y, Dhikuda H, Fukuda A, Wakeyama H,Yasuda H, Nakamura K, Oda H, Miyazaki T, Tanaka S	Identification of an alternatively spliced variant of Ca2+-promoted Ras inactivator as a possible regulator of RANKL shedding.	J Biol Chem.	16	41700-41706	2005
Tanaka S, Nakamura K, Takahashi N, Suda T	Role of RANKL in physiological and pathological bone resorption and therapeutics targeting the RANKL-RANK signaling system.	Immunol Rev	208	30-49	2005
Akiyama T, Miyazaki T, Bouillet P, Nakamura K, Strasser A, Tanaka S.	In vitro and in vivo assays for osteoclast apoptosis.	Biol Proced Online	7	48-59	2005
Matsuyama J, Ohnishi I, Sakai R,Suzuki H, Harada A, Besshi M, Masumoto T, Nakamura K	A new method for measurement of bone deformation by echo tracking.	Med Eng Phys	26		2005
Fukuda A, Hikita A, Wakeyama H, Akiyama T, Oda H, Nakamura K, Tanaka S	Regulation of osteoclast apoptosis and motility by small GTPase binding protein Rac1.	J Bone Miner Res	20	2245-2253	2005
Mototani H, Mabuchi A, Saito S, Fujioka M, Iida A, takatori Y, Kotani A,Kubo T,Nakamura K, Sekine A, Murakami Y、Tsunoda T, Notoya K, Nakamura Y,Ikegawa S	A functional single nucleotide polymorphism in the core promoter region of CALM1 is associated with hip osteoarthritis in Japanese.	Hum Mol Genet	14	1009-1017.	2005
Kizawa H,KouI,Iida A, Sudo A,Miyamoto Y, Fukuda A, Mabushi A,Kotani A,Kawakami A,Ymamoto S, Ushida A, Nakamura K, Kotoya K, Nakamura Y, Ikegawa S	An aspartic acid repeat polymorphism in asporin inhibits chondrogenesis and increases susceptibility to osteoarthritis.	Nat Genet	37	138-144.	2005
Yosihmura N, Suzuki T, Hosoi T, Orimo H	Epidemiology of hip fracture in Japan: Incidence and risk factors.	J Bone Miner Metab	23 suppl	78-80	2005
Fujiwara S, Sone T, Yamazaki K, Yoshimura N, Nakatuska K, Masunari N, Fujita S, Kushida K, Fukunaga M	Heel Bone Ultrasound Predicts Non-spine Fracture in Japanese Men and Women.	Osteopoos Int	16	2107-2112	2005
Chikuda H, Kugimiya F, Hoshi K, Ikeda T, Ogasawara T, Kamekura S, Ogata N, Nakamura K, Chung UI, and Kawaguchi H	Mutation in cGMP-dependent protein kinase II causes dwarfism in a rat mutant KMI through uncoupling of proliferation and differentiation of chondrocytes.	Bone Miner Metab	23	200-204	2005

Takeshita K, Seichi A, Akune T, Kawamura N, Kawaguchi H, and Nakamura K	Can laminoplasty maintain the cervical alignment even when the C2 lamina is contained.	Spine	30	1294-1298	2005
Anamizu Y, Kawaguchi H, Seichi A, Yamaguchi S, Kawakami E, Kanda N, Matsubara S, Kuro-o M, Nabeshima Y, Nakamura K, and Oyanagi K	*Klotho* insufficiency causes decrease of ribosomal RNA gene transcription activity, cytoplasmic RNA and rough ER in the spinal anterior horn cells.	Acta Neuropathol	109	457-66	2005
Yamaguchi M, Ogata N, Shinoda Y, Akune T, Kamekura S, Terauchi Y, Kadowaki T, Hoshi K, Chung UI, Nakamura K, and Kawaguchi H	Insulin receptor substrate-1 is required for bone anabolic function of parathyroid hormone in mice.	Endocrinology	146	2620-2628	2005
Kawaguchi H, Akune T, Yamaguchi M, Ohba S, Ogata N, Chung UI, Kubota N, Terauchi Y, Kadowaki T, and Nakamura K	Distinct effects of PPARgannma insufficiency on bone marrow cells, osteoblasts, and osteoclastic cells.	J Bone Miner Metab	23	275-279	2005
Yano F, Kugimiya F, Ohba S, Ikeda T, Chikuda H, Ogasawara T, Ogata N, Takato T, Nakamura K, Kawaguchi H, Chung UI	The canonical Wnt signaling pathway promotes chondrocyte differentiation in a Sox9-dependent manner.	Biochem Biophys Res Commun	333	1300-1308	2005
Moro T, Ogasawara T, Chikuda H, Ikeda T, Ogata N, Maruyama Z, Komori T, Hoshi K, Chung UI, Nakamura K, Okayama H, and Kawaguchi H	Inhibition of Cdk6 expression through p38 MAP kinase is involved in differentiation of mouse prechondrocyte ATDC5.	J Cell Physiol	204	927-933	2005
Kamekura S, Hoshi K, Shimoaka T, Chung UI, Chikuda H, Yamada T, Uchida M, Ogata N, Seichi A, Nakamura K, and Kawaguchi H	Osteoarthritis development in novel experimental mouse models induced by knee joint instability.	Osteoarthritis Cartilage	13	632-641	2005
Seichi A, Takeshita K, Nakajima S, Akune T, Kawaguchi H, Nakamura K:	Revision cervical spine surgery using transarticular or pedicular screws under a computer-assisted image-guidance system.	J Orthop Sci	10	385-390	2005
Seichi A, Takeshita K, Kawaguchi H, Kawamura N, Higashikawa A, and Nakamura K	Image-guided surgery for thoracic ossification of the posterior longitudinal ligament	J Neurosurg Spine	3	165-168	2005
Ikeda T, Kawaguchi H, Kamekura S, Ogata N, Mori Y, Nakamura K, Ikegawa S, and Chung UI	Distinct roles of SOX5, SOX6 and SOX9 in different stages of chondrogenic differentiation.	J Bone Miner Matab	23	337-340	2005

Kurosu H, Yamamoto M, Clark JD, Pastor JV, Nandi A, Gurnani P, McGuinness OP, Chikuda H, Yamaguchi M, Kawaguchi H, Shimomura I, Takayama Y, Herz J, Kahn CR, Rosenblatt KP, and Kuro-o M	Suppression of aging in mice by the hormone Klotho.	Science	309	1829-1833	2005
Kugimiya F, Kawaguchi H, Kamekura S, Chikuda H, Ohba S, Yano F, Ogata N, Katagiri T, Harada Y, Azuma Y, Nakamura K, and Chung UI	Involvement of endogenous bone morphogenetic protein (BMP)2 and BMP6 in bone formation.	J Biol Chem	280	35704-35712	2005
Kugimiya F, Yano F, Ohba S, Igawa K, Nakamura K, Kawaguchi H, and Chung UI	Mechanism of osteogenic induction by FK506 via BMP/Smad pathways.	Biochem Biophys Res Commun	338	872-879	2005
Masuda H, Chikuda H, Suga T, Kawaguchi H, and Kuro-o M	Regulation of multiple ageing-like phenotypes by inducible *klotho* gene expression in klotho mutant mice.	Mech Ageing Dev	126	1274-1283	2005
Kugimiya F, Chikuda H, Kamekura S, Ikeda T, Hoshi K, Ogasawara T, Nakamura K, Chung UI, and Kawaguchi H	Involvement of cyclic quanosine monophosphate-dependent protein kinase II in chondrocyte hypertrophy during endochondral ossification.	Mod Rheumatol	15	391-396	2005
Takahashi T, Ogasawara T, Kishimoto J, Liu G, Asato H, Nakatsuka T, Uchinuma E, Nakamura K, Kawaguchi H, Takato T, and Hoshi K	Synergistic effects of FGF-2 with insulin or IGF-I on the proliferation of human auricular chondrocytes.	Cell Transplant	14	683-693	2005
R. Ideta, F. Tasaka, W. -D. Jang, N. Nishiyama, G. -D. Zhang, A. Harada, Y. Yanagi, Y. Tamaki, T. Aida, K. Kataoka,	Nanotechnology-based photodynamic therapy for neovascular disease using a supramolecular nanocarrier loaded with a dendritic photosensitizer.	Nano Lett.	5 (12)	2426-2431	2005
K. Miyata, Y. Kakizawa, N. Nishiyama, Y. Yamasaki, T. Watanabe, M. Kohara, K. Kataoka,	Freeze-dried formulations for in vivo gene delivery of PEGylated polyplex micelles with disulfide crosslinked cores to the liver.	J. Control. Release	109 (1-3)	15-23	2005
N. Nishiyama, A. Iriyama, W. -D. Jang, K. Miyata, K. Itaka, Y. Inoue, H. Takahashi, Y. Yanagi, Y. Tamaki, H. Koyama, K. Kataoka,	Light-induced gene transfer from packaged DNA enveloped in a dendrimeric photosensitizer.	Nat. Mater	4 (12)	934-941	2005
X. Yuan, Y. Yamasaki, A. Harada, K. Kataoka,	Characterization of stable lysozyme-entrapped polyion complex (PIC) micelles with crosslinked core by glutaraldehyde.	Polymer	46 (18)	7749-7758	2005

Y. Bae, W. -D. Jang, N. Nishiyama, S. Fukushima, K. Kataoka,	Multifunctional polymeric micelles with folate-mediated cancer cell targeting and pH-triggered drug releasing properties for active intracellular drug delivery.	Molecular BioSystems	1 (3)	242-250	2005
K. Osada, Y. Yamasaki, S. Katayose, K. Kataoka, A	synthetic block copolymer regulates S1 nuclease fragmentation of supercoiled plasmid DNA. Angew.	Chem. Int. Ed. Engl	44 (23)	3544-3548	2005
S. Fukushima, K. Miyata, N. Nishiyama, N. Kanayama, Y. Yamasaki, K. Kataoka,	PEGylated polyplex micelles from triblock cationers with spatially ordered layering of condensed pDNA and buffering units for enhanced intracellular gene delivery.	Am. Chem. Soc	127 (9)	2810-2811	2005
X. Yuan, A. Harada, Y. Yamasaki, K. Kataoka,	Stabilization of lysozyme-incorporated polyion complex micelles by the ω-end derivatization of poly(ethylene glycol)-poly(α , β -aspartic acid) block copolymers with hydrophobic groups.	Langmuir	21 (7)	2668-2674	2005
S. Takae, Y. Akiyama, H. Otsuka, T. Nakamura, Y. Nagasaki, K. Kataoka,	Ligand density effect on biorecognition by PEGylated gold nanoparticles: regulated interaction of RCA120 lectin with lactose installed to the distal end of tethered PEG strands on gold surface.	Biomacromolecules	6 (2)	818-824	2005
Y. Bae, N. Nishiyama, S. Fukushima, H. Koyama, Y. Matsumura, K. Kataoka,	Preparation and biological characterization of polymeric micelle drug carriers with intracellular pH-triggered drug release property: Tumor permeability, controlled subcellular drug distribution, and enhanced in vivo antitumor efficacy.	Bioconjug. Chem.	16 (1)	122-130	2005
W. -D. Jang, N. Nishiyama, G. -D. Zhang, A. Harada, D. -L. Jiang, S. Kawauchi, Y. Morimoto, M. Kikuchi, H. Koyama, T. Aida, K. Kataoka,	Supramolecular nanocarrier of anionic dendrimer porphyrins with cationic block copolymers modified with poly(ethylene glycol) to enhance intracellular photodynamic efficacy. Angew.	Chem. Int. Ed. Engl.	44 (3)	419-423	2005
H. Cabral, N. Nishiyama, S. Okazaki, H. Koyama, K. Kataoka,	Preparation and biological properties of dichloro(1,2-diaminocyclohexane) platinum(II) (DACHPt)-loaded polymeric micelles.	J. Control. Release	101 (1-3)	223-232	2005
Tanaka K, Mori T, Juji T, Suzuki S, Watanabe J, Goto A, Shiobara N, Yamane S, Fukui N, Suzuki R, Ochi T.	Production of interleukin-6 and interleukin-8 by nurse-like cells from rheumatoid arthritis patients after stimulation with monocytes.	Mod Rheumatol	15	415-422	2005
Watanabe A, Wada Y, Obata T, Sasho T, Ueda T, Tamura M, Ikehira H, Moriya H	Time course evaluation of reparative cartilage with MR imaging after autologous chondrocyte implantation.	Cell Transplantation	14(9)	695-700	2005

Watanabe A, Wada Y, Obata T, Sasho T, Ueda T, Tamura M, Ikehira H, Moriya H	Time course evaluation of reparative cartilage with MR imaging after autologous chondrocyte implantation.	Cell Transplantation	14(9)	695-700	2005
Hotta H. Yamada H. Takaishi H. Abe T. Morioka H. Kikuchi T. Fujikawa K. Toyama Y.	Type II collagen synthesis in the articular cartilage of a rabbit model of osteoarthritis: expression of type II collagen C-propeptide and mRNA especially during early-stage osteoarthritis.	Journal of Orthopaedic Science	10(6)	595-607	2005
吉村典子	骨粗鬆症のEBM ：2.骨粗鬆症による椎体・非椎体骨折の生命予後のEBM.	医学のあゆみ	212	143-148	2005
吉村典子	骨粗鬆症と骨折の医療・社会的影響.	日本内科学会雑誌	94	619-625	2005
吉村典子	骨を守る生活習慣を学ぶ	ホルモンと臨床	53	449-454	2005
吉村典子	生活習慣介入による骨折・骨粗鬆症予防についての勧告（運動・喫煙・飲酒）	Clinical Calcium	15	1399-1408	2005
吉村典子	男性の骨粗鬆症診断・治療のピットフォールとは？	骨粗鬆症治療	4	217-223	2005
吉村典子、岡敬之	日本における骨粗鬆症のリスクファクターの考え方-欧米との比較も含めて.	Clinical Calcium	15	1457-1462	2005
吉村典子、中塚喜義、中村利孝、折茂肇	骨粗鬆症の病型分類の考え方-Back to Albright	Osteoporos Jpn	13	839-845	2005
佐粧孝久、和田佑一、田原正道、守屋秀繁	OAに対する鏡視下内側解離術の適応に対する考察	東日本整形災害外科学会誌	17(2)	151-5	2005
山田治基、杉本春夫、金治有彦	ヒアルロン酸製剤の関節内注入療法の効果について	リウマチ科	34(3)	317-326	2005
Oda H, Nakamura K, Matsushita T,Ymamoto S, Ishibashi H, Ymazaki T ,Morimoto S	Clinical use of a newly developed calcium phosphate cement (XSB-671D).	J Orthop Sci	11	167-174	2006
Katagiri M, Ogasawara T, Hoshi K, Chikazu D, Kimoto A, Noguchi M, Sasamata M, Harada S, Akama H, Tazaki H, Chung UI, Takato T, Nakamura K, and Kawaguchi H	Suppression of adjuvant-induced arthritic bone destruction by cyclooxygenase-2 selective agents with and without inhibitory potency against carbonic anhydrase II	J Bone Miner Res	21	219-227	2006
Muraki S,Yamamoto S,Ishibashi H, Nakamura K	Factors associated with mortality following hip fracture in Japan.	J Bone Miner Metab	24	100-104	2006
Ogata T, Ymamoto S, Nakamura K, Tanaka S	Signaling axis in schwann cell proliferation and differentiation.	Mol Neurobiol	33	51-62	2006

Katagiri M, Ogasawara T, Hoshi K, Chikazu D, Kimoto A, Noguchi M, Sasamata M, Harada S, Akama H, Tazaki H, Chung UI, Takato T, Nakamura K, and Kawaguchi H	Suppression of adjuvant-induced arthritic bone destruction by cyclooxygenase-2 selective agents with and without inhibitory potency against carbonic anhydrase II.	J Bone Miner Res	21	219-227	2006
Yoshimura N, Kinoshita H, Hori N, Nishioka T, Ryujin M, Mantani Y, Miyake M, Takeshita T, Ichinose M, Yoshiida M, Oka H, Kawaguchi H, Nakamura K, Cooper C	Risk factors for knee osteoarthritis in Japanese men: A case control study.	Modern Rheumatology	16	24-29	2006
Kugimiya F, Ohba S, Nakamura K, Kawaguchi H, and Chung UI	Physiological role of bone morphogenetic proteins in osteogenesis.	J Bone Miner Metab	24	95-99	2006
Tashiro T, Hiraoka H, Ikeda Y, Ohnuki T, Suzuki R, Ochi T, Nakamura K, Fukui N.	Effect of GDF-5 on ligament healing.	J Orthop Res	24(1)	71-79	2006
Hiraoka H, Kuribayashi S, Fukuda A, Fukui N, Nakamura K.	Endoscopic anterior reconstruction using acomputer-assisted fluoroscopic navigation system.	J Orthop Sci	11(2)	159-166	2006
Sano S, Okawa A, Nakajima A, Tahara M, Fujita K, Wada Y, Yamazaki M, Moriya H, Sasho T	Identification of Pip4k2beta as a mechanical stimulus responsive gene and its expression during musculoskeletal tissue healing.	Cell Tissue Res	323(2)	245-52	2006
Sakai H, Sasho T, Wada Y, Sano S, Iwasaki J, Morita F, Moriya H.	MRI of the popliteomeniscal fasciculi.	Am J Roentgenol	186(2)	460-6	2006

III. 研究成果の刊行物・別刷①

（平成１９年度分）

Colloid Polym Sci (2007) 285:1055–1060
DOI 10.1007/s00396-007-1660-6

SHORT COMMUNICATION

pH-Responsive PEGylated nanogels as targetable and low invasive endosomolytic agents to induce the enhanced transfection efficiency of nonviral gene vectors

Motoi Oishi · Hisato Hayashi · Keiji Itaka · Kazunori Kataoka · Yukio Nagasaki

Received: 18 December 2006 / Accepted: 3 February 2007 / Published online: 28 February 2007

Abstract A pH-responsive PEGylated nanogel was successfully prepared by means of emulsion copolymerization of 2-(*N*,*N*-diethylamino)ethyl methacrylate (AMA) with heterobifunctional poly(ethylene glycol) (PEG) bearing a 4-vinylbenzyl group at the α-end and a lactose moiety at the ω-end in the presence of potassium persulfate and ethyleneglycol dimethacrylate as a cross-linker. Polyplex micelle composed of PEG-*block*-poly(L-lysine) copolymer and plasmid DNA (PEG-*b*-PLL/pDNA) exhibited a far more efficient transfection ability in the presence of lac-nanogel-8k-1.0% (PEG, M_n=8000; cross-linking density, 1.0%) than the PEG-*b*-PLL/pDNA polyplex micelle alone (in the absence of lac-nanogel-8k-1.0%), suggesting that an appreciable fraction of lac-nanogel-8k-1.0% along with the PEG-*b*-PLL/pDNA polyplex micelle is taken up into the HuH-7 cells through the asialoglycoprotein receptor-mediated endocytosis process mediated by the cluster of a large number of lactose moieties on the surface of lac-nanogel-8k-1.0%, followed by the effective disruption of the endosome by the buffer effect of the unprotonated PAMA core in lac-nanogel-8k-1.0%.

Keywords Core-shell type nanogel · pH-sensitive volume phase transition · Endosomolytic agent · Gene vector · PEG-tethering surface

Electronic supplementary material The online version of this article (doi:10.1007/s00396-007-1660-6) contains supplementary material, which is available to authorized users.

M. Oishi · Y. Nagasaki
Tsukuba Research Center for Interdisciplinary Materials Science (TIMS), University of Tsukuba,
1-1-1 Ten-noudai,
Tsukuba, Ibaraki 305-8573, Japan

M. Oishi · H. Hayashi · Y. Nagasaki (✉)
Graduate School of Pure and Applied Sciences,
University of Tsukuba,
1-1-1 Ten-noudai,
Tsukuba, Ibaraki 305-8573, Japan
e-mail: nagasaki@nagalabo.jp

K. Itaka · K. Kataoka
Division of Clinical Biotechnology,
Center for Disease Biology and Integrative Medicine,
Graduate School of Medicine,
The University of Tokyo,
7-3-1 Hongo, Bunkyo-ku,
Tokyo 113-0033, Japan

K. Kataoka
Department of Materials Engineering,
Graduate School of Engineering, The University of Tokyo,
7-3-1 Hongo, Bunkyo-ku,
Tokyo 113-8656, Japan

Introduction

Nonviral gene delivery systems have recently received increased attention in the field of gene therapy in vivo and ex vivo because of concerns over safety issues related to viral vectors, including immunogenicity, oncogenicity, and potential virus recombination [1–3]. Most of the nonviral vectors developed so far, however, have shown a low transfection efficiency compared to viral vectors because the latter have evolved a multifunctionality, which overcomes one of the critical barrier to efficient gene delivery by enhancing transport to the cytoplasm from the endosomal compartment. Recently, a new class of nonviral gene vectors has been developed based on the supramolecular assembly between plasmid DNA (pDNA) and poly(ethylene glycol) (PEG)-*block*-polyamine copolymers (polyplex micelles) [4–10]. Due to the highly dense PEG shell surrounding the polyion complex (PIC) core, the polyplex

micelles with a size of less than 100 nm exhibited excellent solubility in aqueous media, low cytotoxicity, high tolerability toward nuclease degradation, and minimal interaction with biological components, including proteins and cells, compared to conventional polyplex and lipoplex systems.

Nevertheless, the presence of 100 μM hydroxychloroquine (HCQ) as an endosomolytic agent has so far been required to achieve a high transfection efficiency [2, 11], indicating that endosomal escape should be the most critical barrier to intracellular gene delivery by polyplex micelles [12, 13]. To devise polyplex micelles with a function to escape from the endosome where the pH is 1.4~2.4 units lower than the physiological pH of 7.4 [14–17], poly (ethylenimine) (PEI) derivatives are of interest as an alternative way to accomplish endosomal escape by taking advantage of their substantially lowered value of apparent pK_a (~5.5; "buffer or proton-sponge effect") [18]. However, the buffer effect of the PEI segment occurs only when an excess of amino groups with respect to DNA phosphate groups (high N/P ratio) is present in the system, where a considerable amount of the amino groups in PEI is in free-base form. This fact strongly suggests that free PEI, which is not complexed with pDNA, is likely to play a crucial role in the buffer effect [19, 20]. In addition, both HCQ and free PEI tend to show high toxicity and nonspecific disposition in the body after intravenous injection, viz., the use of HCQ and PEI for the gene therapy under in vitro and ex vivo conditions is still controversial. A major key to the success of nonviral gene delivery system is believed to be the development of targetable and low invasive endosomolytic agents, which can achieve the low cytotoxicity and modulated disposition in the body as well as the smooth accumulation into the target cell.

Worth noting in this regard is a new class of pH-responsive PEGylated nanogels constructed from a cross-linked pH-sensitive polyamine core and tethered PEG chains bearing a carboxylic acid group as a platform moiety to install ligand molecules [21]. The pH-responsive nanogels showed excellent stability under physiological conditions and significant volume phase transition (swelling) in response to endosomal pH (pH>7.5, diameter ca. 80 nm; pH<6.5, diameter ca. 150 nm; see Fig. S1) due to the protonation of the cross-linked polyamine core surrounded by the tethered PEG chains, indicating that the cross-linked polyamine core of the nanogels acts as a buffering moiety for facilitated endosomal escape. A unique finding, which we would like to communicate in this paper, is the remarkably enhanced transfection efficiency without cytotoxicity in cultured hepatoma cells through the PEGylated polyplex micelle composed of PEG-*block*-poly (L-lysine) copolymer (PEG-*b*-PLL: $M_{n\ PEG}$=12,000, $M_{n\ PLL}$=11,600) and pDNA along with pH-responsive lactosylated nanogel (Fig. 1); thus, the pH-responsive lactosylated nanogel is promising as a targetable and

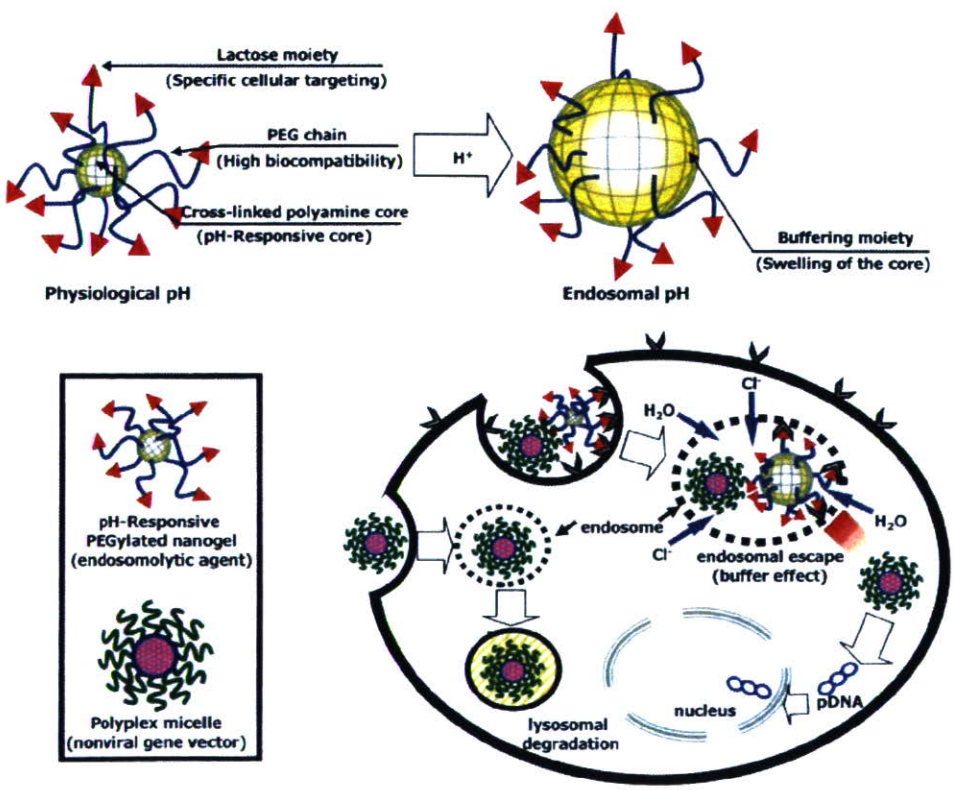

Fig. 1 Schematic illustration of the pH-responsive PEGylated nanogel and endosomal escape mechanism

biocompatible endosomolytic agent for nonviral gene delivery systems.

Experimental

General Ethylene glycol dimethacrylate (EGDMA; Wako) and 2-(*N,N*-diethylamino)ethyl methacrylate (AMA, Wako) were distilled over CaH_2 under reduced pressure. Potassium persulfate (KPS; Wako) was purified by recrystallization from water and then dried in vacuo. Asialofetuine (ASF) and HCQ were purchased from Sigma and Acros Organics, respectively. Water was purified using the Milli-Q system (Millipore). Plasmid DNA (pDNA) encoding firefly luciferase (pGL3-Luc, Promega; 5,256 bpa) was amplified using EndoFree™ Plasmid Maxi or Mega Kits (Qiagen). The DNA concentration was determined by reading the absorbance at 260 nm. Dynamic light scattering (DLS) measurements were carried out using a light-scattering spectrometer (DLS-7000, Otsuka Electronics. Japan) equipped with a vertically polarized incident beam at 488 nm supplied by an argon ion laser at scattering angles of 90°. Lasser–Doppler electrophoresis measurements of the PEGylated nanogels were carried out in 10 mM $NaCl_{aq}$ (ELS-600, Photal, Otsuka Electronics).

Synthesis of CH_2=CH–Ph–PEG–lactose and preparation of nanogels Heterobifunctional α-vinylbenzyl-ω-carboxyl-poly(ethylene glycol) [CH_2=CH–Ph–PEG–COOH; molecular weights (MW): 2k and 8k] macromonomers were synthesized in accordance with our previous report [21]. To a solution of potassium 4-vinylbenzyl alcoholate (0.5 mmol) in tetrahydrofolate (THF; 20 ml), 22.7 mmol (1.1 ml) of ethylene oxide were added under an argon atmosphere. After the reaction mixture was stirred at room temperature for 2 days, 2.5 mmol (3.4 ml, 0.725 mol/l in THF solution) of succinic anhydride was added to introduce a carboxylate group at the ω-end. After the purification of CH_2=CH–Ph–PEG–COOH, lactose was installed at the carboxylic acid group of CH_2=CH–Ph–PEG–COOH through an activated ester method, viz., 8.0 mg of CH_2=CH–Ph–PEG–COOH (MW: 8k, 10 μmol) were reacted with 22 mg of *p*-aminophenyl-β-D-lactopyranoside (50 μmol) in the presence of 250 μmol of *N*-hydroxysuccinimide (NHS) and 1.25 mmol of 1-ethyl-3-(3-dimethylaminopropyl)carbodiimide, hydrochloride (EDC; NHS/EDC ratio of 1:5) in 25 mM 2-morpholinoethanesulfonic acid (MES) buffer (10 ml), pH 6.5. The reaction mixture was stirred at room temperature for 24 h. The CH_2=CH–Ph–PEG–lactose was precipitated in cooled 2-propanol (twice) and dialyzed (MWCO: 3,500) against distilled water for 2 days. The CH_2=CH–Ph–PEG–lactose was finally freeze-dried from water to quantitatively obtain the white powder. We used a typical procedure for the preparation of the pH-responsive nanogels possessing a lactose moiety at the PEG chains, as follows: after 65 mg (8.1 μmol) of the obtained CH_2=CH–Ph–PEG–lactose (8k) were loaded into the reactor, the vacuum and argon purging cycles were repeated three times, followed by the successive addition of deionized/distilled water (1.5 ml), 130 μg of 2-(*N,N*-diethylamino) ethyl methacrylate (AMA, 141 μl, 700 μmol) and 1.5 μl of ethyleneglycol dimethacrylate (EGDMA, 7.1 μmol). Emulsion copolymerization was initiated with the addition of 1 ml of aqueous KPS (7.2 mM). The mixture was allowed to react at room temperature for 24 h with stirring. The nanogel was purified by dialysis against distilled water for 2 days.

Cytotoxicity assay Human hepatocarcinoma cells (HuH-7) were seeded onto 96-well plates at a seeding density of 8×10^3 cells/well. The cells were maintained in Dulbecco's modified Eagle's medium (DMEM) supplemented with 10% fetal bovine serum (FBS) and 1.0% penicillin–streptomycin for 24 h at 37 °C in a humidified atmosphere under 5% CO_2. Then, the culture medium was replaced by 90 μl of fresh medium containing serum and antibiotic, followed by the addition of 10 μl of the nanogels at various concentrations. After 24 h, 100 μl of 3-(4,5-dimethylthiazol-2-yl)-2,5-diphenyl tetrazolium bromide (MTT assay, cell counting kit; Dojindo) stock solution in culture medium were added to each well. After an additional 4 h of incubation, the viability of the cells in each well was measured following the protocol provided by the manufacturer. The results are expressed as means±SEM, $n=8$.

Transfection study To a pDNA (pGL3-Luc, Promega; 5,256 bps) solution in 10 mM Tris–HCl buffer (pH 7.4), PEG-*block*-poly(L-lysine) (PEG-*b*-PLL: $M_{n\ PEG}$=12,000, $M_{n\ PLL}$=11,600), the block copolymer solution in the same buffer, was added at the charge ratio of lysine units vs nucleotide equals 2 (N/P=2) to prepare the polyplex micelle. The HuH-7 cells were seeded in 24-well culture plates at a seeding density of 2.5×10^4 cells/well. After a 24-h incubation in a medium containing 10% FBS, the cells were rinsed, and then 250 μl of the culture medium containing 100 μg/ml of lac-nanogel-8k along with the PEG-*b*-PLL/pDNA polyplex micelle solution (25 μl/well; pDNA concentration, 30 μg/ml) were added to each well. After 24 h, the medium was removed and then replaced with the culture medium. The luciferase gene expression was measured after a further 24 h of culturing. For the competitive inhibition assay of lac-nanogel-8k to the asialoglycoprotein (ASGP) receptor on the HuH-7 cells, a medium containing 1.5 mg/ml of ASF was added to the culture system 30 min before the transfection study. The cells were lysed, and the luciferase activity of the lysate

was monitored with a Luciferase Assay Kit (Promega) and luminometer (Lumat LB 9507, Berthold). The results were expressed as light units per milligram of cell protein determined by a micro BCA assay kit (Pierce).

Results and discussion

Heterobifunctional PEGs bearing 4-vinylbenzyl group at the α-end and a carboxylic acid at the ω-end (CH_2=CH–Ph–PEG–COOH, M_n=1,800 and 8,000) were synthesized, in accordance with our literature [21]. The introduction of a lactose group to the carboxylic acid end of CH_2=CH–Ph–PEG–COOH (M_n=8,000) was performed by the reaction with *p*-aminophenyl-β-D-lactopyranoside in the presence of an excess amount of NHS and EDC in 25 mM MES buffer, pH 6.5, at room temperature for 24 h. Based on the hydrogen nuclear magnetic resonance (^{1}H NMR) spectrum of CH_2=CH–Ph–PEG–lactose (Fig. 2), the lactose molecules were almost quantitatively introduced to the PEG chain end as determined by the integral ratio between the ester metylene protons (4.1 ppm, 2H, PEG–CH_2CH_2–O–CO–CH_2–) and the phenyl protons of the lactose moiety (6.9 ppm, 2H, –CO–NH–Ph–lactose). Lactosylated and nonlactosylated nanogels were prepared at room temperature by means of the emulsion polymerization of 2-(*N,N*-diethylamino)ethyl methacrylate (AMA) with CH_2=CH–Ph–PEG–lactose (M_n=8,000) or CH_2=CH–Ph–PEG–COOH (M_n=1,800 or 8,000) in the presence of KPS and EGDMA (0.1 or 1 mol%) as a cross-linker because the tertiary amino groups in the AMA monomer and KPS spontaneously forms a redox complex (initiator) at room temperature through the electron transfer from AMA to KPS. The characterizations of the obtained nanogels with a unimodal size distribution (μ_2/Γ^2<0.15) are summarized in Table 1.

An MTT assay was done using HuH-7 cells (human hepatoma cells) possessing ASGP receptors, which recognize compounds bearing terminal galactose moieties [22, 23], to evaluate the cytotoxicity of the obtained nanogels, as shown in Fig. 3. Nanogel-2k-1.0% with short PEG chains (M_n=1,800) and nanogel-8k-0.1% with low cross-linking density showed high cytotoxicity in a dose-dependent manner, despite possessing PEG chains surrounding the cross-linked PAMA core: The 50% cytotoxicity concentrations were determined to be ca. 10 and 6 μg/ml, respectively. In addition, the viability of cells treated with HCQ was less than 50% at 100 μM (=31.4 μg/ml). In sharp contrast, nanogel-8k-1.0% and lac-nanogel-8k-1.0% with long PEG chains (M_n=8,000) and moderate cross-linking density (1.0%) showed low cytotoxicity even at 100 μg/ml (>70% cell viability). These results suggest that the cytotoxicity of the nanogels obviously depended on the chain length of the PEG and the cross-linking density of the PAMA core. The observed high cytotoxicity of nanogel-2k-1.0% and nanogel-8k-0.1% is most likely due to partial exposure of the PAMA core to the outside and/or the existence of dangling PAMA chains, as the zeta potential of the fully protonated nanogel-2k-1.0% and nanogel-8k-0.1% at pH 5 was found to be +32.3 and +33.1 mV, respectively. On the contrary, nanogel-8k-1.0% and lac-nanogel-8k-1.0% with longer PEG

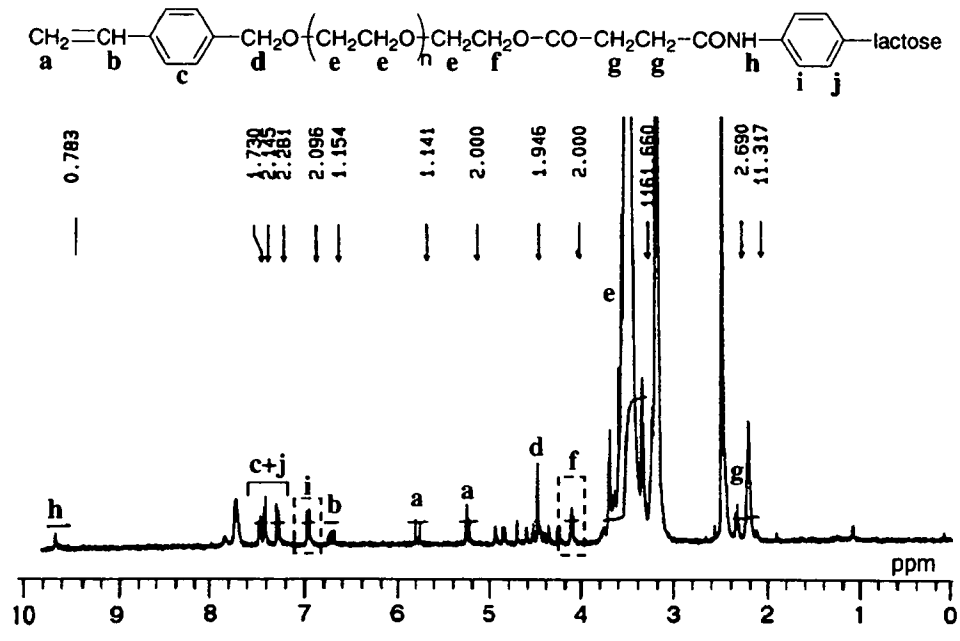

Fig. 2 ^{1}H NMR spectrum of the CH_2=CH–Ph–PEG–lactose in DMSO-d_6 at 55 °C (peaks at 2.5 and 3.2 ppm are attributed to the DMSO and water, respectively)

Table 1 The nanogel samples used in this study

Samples	M_n(PEG)[a]	Cross-linker[b] (mol %)	Particle size[c] (nm)	
			pH 6	pH 8
Nanogel-2k-1.0%	1,800	1.0	128.9	72.0
Nanogel-8k-0.1%	8,000	0.1	320.0	89.3
Nanogel-8k-1.0%	8,000	1.0	152.7	84.4
Lac-nanogel-8k-1.0%	8,000	1.0	160.8	84.7

[a] Determined by SEC chromatography
[b] Feed molar ratio of cross-linking agents: EGDMA
[c] Determined by DLS analysis

chains (M_n=8,000) and higher cross-linking density (1.0%) showed the effective compartmentalization of the cross-linked PAMA core surrounded by long PEG chains to prevent both exposure of the PAMA core to the outside and the formation of dangling PAMA chains (fully protonated nanogel-8k-1.0%, ζ=+14.0 mV), leading to the low cytotoxicity of these nanogels.

To estimate the endosomolytic ability of the nanogels, a transfection study of the PEG-*b*-PLL/pDNA polyplex micelle was carried out in the presence and absence of lac-nanogel-8k-1.0% (100 μg/ml) using HuH-7 cells, although there is no interaction between the polyplex micelle and nanogel due to the existence of the tethered PEG chains (PEG shell). PEG-*b*-PLL/pDNA polyplex micelles were prepared at N/P=2, where the highest transfection efficiency and complete DNA condensation were observed in our previous study [5]. As can be seen in Fig. 4, the PEG-*b*-PLL/pDNA polyplex micelle alone

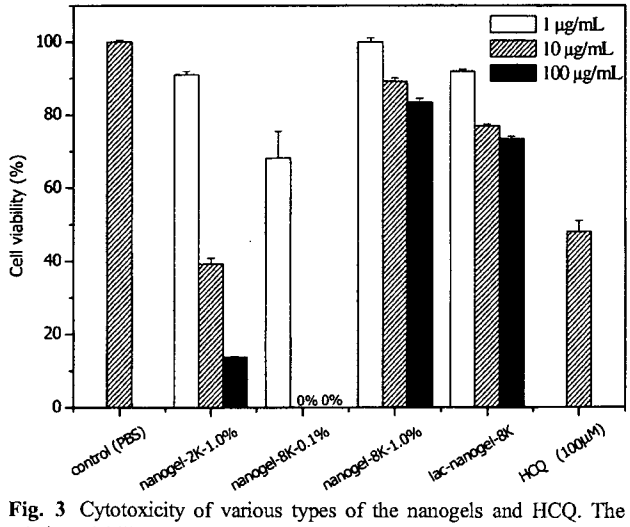

Fig. 3 Cytotoxicity of various types of the nanogels and HCQ. The relative viability of HuH-7 cells is expressed as functions of nanogel concentrations: 1 μg/ml (*open bars*), 10 μg/ml (*gray bars*), and 100 μg/ml (*filled bars*). The results are expressed as means±SEM, n=8

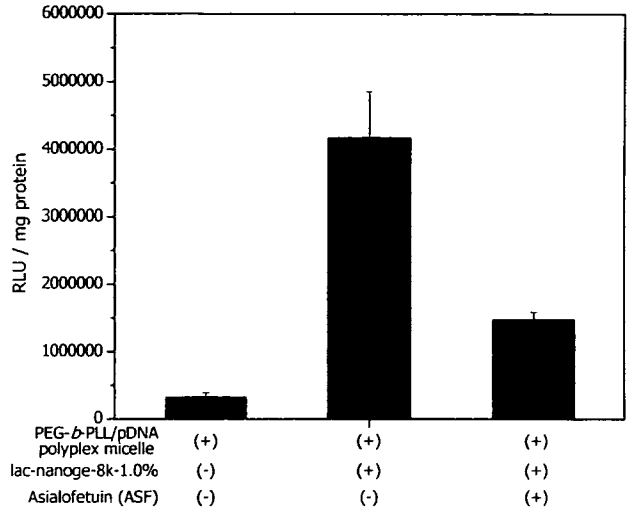

Fig. 4 Efficiency of transfection into HuH-7 cells of the PEG-*b*-PLL/pDNA polyplex micelles prepared at N/P=2. The lac-nanogel-8k-1.0% (100 μg/ml) and ASF (1.5 mg/ml) were used. The results are expressed as means±SEM, n=4

(without lac-nanogel-8k-1.0%) showed only limited transfection efficiency without any cytotoxicity due to the lack of the endosomal escape function, leading to the lysosomal degradation of the pDNA. In sharp contrast, the PEG-*b*-PLL/pDNA polyplex micelle with lac-nanogel-8k-1.0% achieved a significant increase in transfection efficiency compared with the PEG-*b*-PLL/pDNA polyplex micelle alone, viz., the transfection efficiency was found to be 3.2×10^5 (RLU/mg protein) and 4.2×10^6 (RLU/mg protein) for the PEG-*b*-PLL/pDNA polyplex micelle alone and the PEG-*b*-PLL/pDNA polyplex micelle with the lac-nanogel-8k-1.0%, respectively. This almost 13-fold increase in transfection efficiency in lac-nanogel-8k-1.0% is remarkable because other polyplex micelle system in the presence of HCQ (100 μM) showed the 10- and 15-fold enhancement of the transfection efficiency for the HuH-7 cells (same cell line) [19] and HepG2 cells [4], respectively. In addition, significant increase in the transfection efficiency of the PEG-*b*-PLL/pDNA polyplex micelle with nanogel-8k-1.0% was also observed for 293T cells (human kidney; see Fig. S2). These results suggest that after the partial co-internalization of the PEG-*b*-PLL/pDNA polyplex micelle and lac-nanogel-8k-1.0% into the HuH-7 cells, the protonation of the PAMA core of lac-nanogel-8k-1.0% occurred in synchronously with the pH decrease in the endosomal compartment (pH=6~5), leading to the significant swelling of the PAMA core of lac-nanogel-8k-1.0% (pH=8.0, 84.7 nm → pH=6.0, 160.8 nm in Table 1) to increase the ion osmotic pressure (buffer effect). This may induce the disruption of the endosome, facilitating the transport of the co-internalized PEG-*b*-PLL/pDNA polyplex micelle into the cytoplasm.

To examine whether the lactose moiety (galactose terminal) on the surface of lac-nanogel-8k-1.0% is recognized by the ASGP receptors existing on the HuH-7 cells, a transfection study of the PEG-*b*-PLL/pDNA polyplex micelle with lac-nanogel-8k-1.0% was also performed in the presence of ASF. Note that the ASF is known to strongly interact with ASGP receptors, viz., ASF acts as a competitive inhibitor of the ASGP receptor-mediated endocytosis [24]. A significant decrease in the transfection efficiency of the PEG-*b*-PLL/pDNA polyplex micelle with lac-nanogel-8k-1.0% was observed in the presence of ASF, indicating that the cellular association and internalization of lac-nanogel-8k-1.0% along with the PEG-*b*-PLL/pDNA polyplex micelle occur mainly through the ASGP receptor-mediated process, which is inhibited in the presence of ASF. Thus, it seems reasonable to conclude that an appreciable fraction of the lac-nanogel-8k-1.0% along with the PEG-*b*-PLL/pDNA polyplex micelle is taken up by HuH-7 cells through the ASGP receptor-mediated endocytosis process mediated by the cluster of a large number of lactose moieties on the surface of the lac-nanogel-8k-1.0%, followed by the effective disruption of the endosome by the buffer effect of the unprotonated PAMA core in lac-nanogel-8k-1.0%.

In conclusion, the pH-responsive and targetable PEGylated nanogel (lac-nanogel-8k-1.0%) constructed from a cross-linked polyamine core and tethered PEG chains bearing a lactose molecule exhibited significant endosomolytic ability, achieving the pronounced transfection efficiency of the PEG-*b*-PLL/pDNA polyplex micelles without any cytotoxicity. Therefore, the pH-responsive and targetable PEGylated nanogel thus described in this paper would be a promising targetable and biocompatible endosomolytic agent for nonviral gene delivery systems.

References

1. Yang Y, Li Q, Ertl HC, Wilson JM (1995) J Virol 69:2004–2015
2. Yang Y, Li Q, Ertl HC, Wilson JM (1994) Immunity 1:433–442
3. Gunter KC, Khan AS, Noguchi PD (1993) Hum Gene Ther 4:643–645
4. Wakebayashi D, Nishiyama N, Itaka K, Miyata K, Yamasaki Y, Harada A, Koyama H, Nagasaki Y, Kataoka K (2004) Biomacromolecules 5:2128–2136
5. Itaka K, Yamauchi K, Harada A, Nakamura K, Kawaguchi H, Kataoka K (2003) Biomaterials 24:4495–4506
6. Itaka K, Yamauchi K, Harada A, Nakamura K, Kawaguchi H, Kataoka K (2002) Biomacromolecules 3:841–845
7. Harada-Shiba M, Yamauchi K, Harada A, Takamisawa I, Shimokado K, Kataoka K (2002) Gene Ther 9:407–417
8. Kataoka K, Harada A, Wakebayashi D, Nagasaki Y (1999) Macromolecules 32:6892–6894
9. Katayose S, Kataoka K (1998) J Pharm Sci 87:160–163
10. Katayose S, Kataoka K (1997) Bioconjug Chem 8:702–707
11. Wakebayashi D, Nishiyama N, Yamasaki Y, Itaka K, Kanayama N, Harada A, Nagasaki Y, Kataoka K (2004) J Control Release 95:653–664
12. Brown MD, Schatslein AG, Uchegbu IF (2001) Int J Pharm 229:1–21
13. Nishikawa M, Huang L (2001) Hum Gene Ther 12:861–870
14. Gruenberg J (2001) Nat Rev Mol Cell Biol 2:721–730
15. Clague MJ (1998) Biochem J 336:271–282
16. Mukherjee S, Ghosh RN, Maxfield FR (1997) Endocytosis. Physiol Rev 77:759–803
17. Duncan R (1992) Anti-Cancer Drugs 3:175–210
18. Boussif O, Lezoualc F, Zanta MA, Mergny MD, Scherman D, Demeneix B, Behr JP (1995) Proc Natl Acad Sci USA 92:7297–7301
19. Oishi M, Kataoka K, Nagasaki Y (2006) Bioconjug Chem 17:677–688
20. Fukushima S, Miyata K, Nishiyama N, Kanayama N, Yamasaki Y, Kataoka K (2005) J Am Chem Soc 127:2810–2811
21. Hayashi H, Iijima M, Kataoka K, Nagasaki Y (2004) Macromolecules 37:5389–5396
22. Hashida M, Takemura S, Nishikawa M, Takakura Y (1998) J Control Release 53:301–310
23. Stockert RJ (1995) Physiol Rev 75:591–609
24. Zanta MA, Boussif O, Adib A, Behr JP (1997) Bioconjug Chem 8:839–844

Density Control of Poly(ethylene glycol) Layer To Regulate Cellular Attachment

Tomomi Satomi,[†,‡,§,∥] Yukio Nagasaki,[⊥] Hisatoshi Kobayashi,[§] Hidenori Otsuka,[*,†,‡,§] and Kazunori Kataoka[∥,#]

Department of Applied Chemistry, Faculty of Science, Tokyo University of Science, 1-3 Kagurazaka, Shinjuku-ku, Tokyo 162-8601, Japan, Division of Bioengineering and Bioinformatics, Graduate School of Information Science and Technology, Hokkaido University, North 14 West 9, Sapporo 060-0814, Japan, Biomaterials Center, National Institute for Materials Science (NIMS), 1-1 Namiki, Tsukuba, Ibaraki 305-0044, Japan, Division of Clinical Biotechnology, Center for Disease Biology and Integrative Medicine, Graduate School of Medicine, The University of Tokyo, 7-3-1 Hongo, Bunkyo-ku, Tokyo 113-0033, Japan, Graduate School of Pure and Applied Sciences, University of Tsukuba, 1-1-1 Tenodai, Tsukuba, Ibaraki 305-8571, Japan, and Department of Materials Science and Engineering, Graduate School of Engineering, The University of Tokyo, 7-3-1 Hongo, Tokyo 113-8656, Japan

Received August 17, 2006. In Final Form: March 7, 2007

A wide variety of cells usually integrate and respond to the microscale environment, such as soluble protein factors, extracellular matrix proteins, and contacts with neighboring cells. To gain insight into cellular microenvironment design, we investigated two-dimensional microarray formation of endothelial cells on a micropatterned poly(ethylene glycol) (PEG)-brushed surface, based on the relationship between PEG chain density and cellular attachment. The patterned substrates consisted of two regions: the PEG surface that acts as a cell-resistant layer and the exposed substrate surface that promotes protein or cell adsorption. A PEG-brushed layer was constructed on a gold substrate using PEG with a mercapto group at the end of the chain. The density of the PEG-brushed layer increased substantially with repetitive adsorption/rinse cycles of PEG on the gold substrate, allowing marked reduction of nonspecific protein adsorption. These repeated adsorption/rinse cycles were further regulated by using longer (5 kDa) and shorter (2 kDa) PEG to construct PEG layers with different chain density, and subsequent micropatterning was achieved by plasma etching through a micropatterned metal mask. The effects of PEG chain density on pattern formation of cell attachment were determined on micropatterning of endothelial cells. The results indicated that cell pattern formation was strongly dependent on the PEG chain density and on the extent of protein adsorption. Notably, a PEG chain density high enough to inhibit outgrowth of endothelial cells from the cell-adhering region in the horizontal direction could be obtained only by employing formation of a short filler layer of PEG in the preconstructed longer PEG-brushed layer, which prevented nonspecific protein adsorption almost completely. In this way, a completely micropatterned array of endothelial cells with long-term viability was obtained. This clearly indicated the importance of a short underbrushed PEG layer in minimizing nonspecific protein adsorption for long-term maintenance of the active cell pattern. The strategy for cell patterning presented here can be employed in tissue engineering to study cell−cell and cell−surface interactions. It is also applicable for high-throughput screening and clinical diagnostics, as well as interfacing cellular and microfabricated components of biomedical microsystems.

Introduction

Surface engineering techniques for cellular micropatterning are emerging as important tools to clarify the effects of the microenvironment on cellular behavior,[1,2] as cells usually integrate and respond to the microscale environment, such as chemical and mechanical properties of the surrounding fluid and extracellular matrix, soluble protein factors, small signal molecules, and contacts with neighboring cells.[3,4] Furthermore, living cells undergo physiological changes in response to exposure to drugs and environmental perturbations, such as toxins, pathogens, or other agents, and thus high-throughput technologies using whole cells have also been developed.[5−13] To develop this kind of cellular microarray composed of a cell-resistant surface and cell attachment region, micropatterning a protein-repellent surface is important because cellular adhesion and proliferation are regulated by protein adsorption.

* Corresponding author. Address: Hidenori Otsuka, Ph.D., Department of Applied Chemistry, Faculty of Science, Tokyo University of Science, 1-3 Kagurazaka, Shinjuku-ku, Tokyo 162-8601, Japan. Phone: +81-3-5228-8265. Fax: +81-3-5228-8265. E-mail: h.otsuka@rs.kagu.tus.ac.jp.

† Tokyo University of Science.

‡ Hokkaido University.

§ National Institute for Materials Science.

∥ Graduate School of Medicine, The University of Tokyo.

⊥ University of Tsukuba.

Graduate School of Engineering, The University of Tokyo.

(1) Whitesides, G. M.; Ostuni, E.; Takayama, S.; Jiang, X.; Ingber, D. E. *Annu. Rev. Biomed. Eng.* **2001**, *3*, 335.

(2) Jeon, N. L.; Baskaran, H.; Detringer, S. K. W.; Whitesides, G. M.; Van de Water, L.; Toner, M. *Nat. Biotechnol.* **2002**, *20*, 826.

(3) Zamir, E.; Katz, B. Z.; Aota, K. M.; Yamada, K. M.; Geiger, B.; Kam, Z. *J. Cell Sci.* **1999**, *112*, 1655.

(4) Geiger, B.; Bershadsky, R.; Pankov, R.; Yamada, K. M. *Nat. Rev. Mol. Cell Biol.* **2001**, *2*, 793.

(5) Stenger, D. A.; Gross, G. W.; Keefer, E. W.; Shaffer, K. M.; Andreadis, J. D.; Ma, W.; Pancrazio, J. J. *Trends Biotechnol.* **2001**, *19*, 304.

(6) Kononen, J.; Bubendorf, L.; Kallioniemi, A.; Barlund, M.; Schraml, P.; Leighton, S.; Torhorst, J.; Mihatsch, M. J.; Sauter, G.; Kallioniemi, O. P. *Nat. Med.* **1998**, *4*, 844.

(7) Ziauddin, J.; Sabatini, D. M. *Nature* **2001**, *411*, 107.

(8) Michalopoulos, G. K.; DeFrances, M. C. *Science* **1997**, *276*, 60.

(9) Anderson, D. G.; Levenberg, S.; Langer, R. *Nat. Biotechnol.* **2004**, *22*, 863.

(10) Revzin, A.; Tompkins, R. G.; Toner, M. *Langmuir* **2003**, *19*, 9855.

(11) Thielecke, H.; Mack, A.; Robitzki, A. *Biosens. Bioelectron.* **2001**, *16*, 261.

(12) Mack, A. R.; Thielecke, H.; Robitzki, A. A. *Trends Biotechnol.* **2002**, *20*, 56.

(13) Otsuka, H.; Hirano, A.; Nagasaki, Y.; Okano, T.; Horiike, Y.; Kataoka, K. *ChemBioChem* **2004**, *5*, 850.

10.1021/la0624384 CCC: $37.00
Published on Web 05/05/2007

A number of approaches to construct protein-repellent and subsequent cell-repellent surfaces have been studied using polymer coating. In fact, there has been a great deal of discussion regarding the molecular properties on the surface, and it is widely believed that effective protein rejection requires the bound polymer to be heavily hydrated, densely packed, neutral, deposited in a thick layer, and conformationally mobile.[14-18] Here, we focus on poly(ethylene glycol) (PEG), one of the most useful polymers to repel protein. Surface modification by PEG leads to a significant reduction in the nonspecific interaction of biological molecules with the surface due to its high degree of hydrophilicity and chain flexibility, inducing an effective exclusion volume effect.[19-22] Most previous studies of surfaces with immobilized PEG have described higher protein-repellent ability with longer chain, resulting in increasing thickness of PEG,[23-27] which is considered to be due to the stronger attenuation of the long-range Lifshitz−van der Waals attraction. However, immobilization of longer PEG chains results in a decrease in chain density due to its larger exclusion volume effect, although it has a sufficiently large separation between the surface and proteins. Conversely, immobilization of shorter PEG chains gives higher density due to its smaller exclusion volume effect, although it has a smaller separation between the surface and proteins. To resolve this controversial issue of the length and density of the PEG layer, we previously reported the development of surface construction using long and short PEG chains; formation of a short, filler layer of PEG in the preconstructed longer PEG-brushed layer prevented nonspecific protein adsorption almost completely.[28] In most studies of this type, a protein-repellent surface will be expected to repel cellular attachment. However, the question of how dense the immobilized PEG chain must be to control cell attachment has still not been answered.

The present study was performed to determine the influence of PEG chain density on cellular attachment directly. For the micropatterning of cells, it is necessary to prevent overgrowth of cells from the cell-adhering pattern; i.e., construction of a cytophobic surface is important for micropatterning. Here, we controlled the modification ratio of long and short PEG chains to construct surfaces with different PEG chain densities, and subsequent micropatterning was achieved by plasma etching through a micropatterned metal mask (ϕ = 100 μm, edge-to-edge spacing of l = 300 μm). The relationship between PEG chain density and cellular attachment is discussed on micropatterning of endothelial cells.

Experimental Section

Materials. Poly(ethylene glycol) (PEG) with a methoxy group at one end and a mercapto group at the other (MeO−PEG−SH) was provided by NOF Corporation (Tokyo, Japan). The molecular weight and polydispersity of PEGs, denoted by PEG2k and PEG5k, were 2096 and 1.05 and 5341 and 1.04, respectively. Gold chips (SIA KIT Au) for SPR measurements were purchased from Biacore AB (Uppsala, Sweden). Human umbilical endothelial cells (HUVEC) were purchased from Cambrex (Cambrex BioScience Walkersville, Inc., Walkersville, MD). HUVECs were cultured in EBM-2 medium (Cambrex). Water used in this study was purified by passing it through a Milli-Q System (Nihon Millipore Co., Tokyo, Japan) until its specific conductivity fell below 0.1 μS cm^{-1}.

1. PEG Immobilization Study. *Preparation of MeO−PEG−SH-Modified Gold Surface.* Immobilization of PEG on the gold sensor chip surface was performed using a surface plasmon resonance (SPR) instrument (Biacore X; Biacore AB, Uppsala, Sweden). Phosphate buffered saline (PBS; pH 7.4, 0.15 M, containing 1 M NaCl) solutions of PEG were injected at a flow rate of 10 μL/min for 10 min at 37 °C under running PBS (pH 7.4, 0.15 M, containing 1 M NaCl). An SPR sensorgram on the gold sensor chip for this adsorption/rinsing (with running PBS) of PEG was monitored, and the amount of immobilized PEG was assessed by the SPR angle shift. PEG solutions with different concentrations were injected on a sensor chip, and then the plateau region for PEG immobilization was determined. To increase (or change) the amount of immobilized PEG, the process of PEG injection was repeated several times according to the reported method.[24] PEGylated surfaces prepared by one, two, and three repetitive injections were denoted as PEG5k(1), PEG5k(2), and PEG5k(3) surfaces, respectively. In a manner similar to the above-repeated process, successive PEGylation with longer and then shorter PEG was carried out. A shorter PEG (PEG2k) as a filler was layered on the surface with the preconstructed longer PEG brushes (PEG5k) by repetitive injection. PEG5k(1) surfaces with three treatments with the filler PEG and PEG5k(2) with four treatments with the filler PEG were denoted as PEG5k(1)/2k(3) and PEG5k(2)/2k(4) surfaces, respectively.

The density of immobilized PEG chains was estimated quantitatively by quartz crystal microbalance (QCM) measurement using an AT-cut gold-sputtered quartz crystal with a resonance frequency of 27 MHz (Initium Inc., Japan). The frequency was recorded after immersing the crystals in the PBS (pH 7.4, 0.15 M, containing 1 M NaCl) at 37 °C. After baseline stabilization, PEG solutions (PEG5k, PEG2k) were injected at a concentration of 0.01 mg/mL, which was optimized above in the same repetitive manner as in SPR measurement (PEG5k(3), PEG5k(1)/2k(3), PEG5k(2)/2k(4)).

Surface Characterization. The wettability of all PEGylated surfaces was estimated from the static and dynamic contact angle measurements (CA-W contact angle meter; Kyowa Interface Science Co., Ltd., Tokyo, Japan).[29] Gold and PEGylated gold surfaces were constructed on glass substrates as described in detail in the section describing the cell culture study (see "Construction of PEGylated surface"). Water-in-air and air-in-water systems were applied in the static contact angle measurements. Water-in-air system measurement was performed by a sessile droplet technique, where a water droplet (Milli-Q quality) was placed on the sample surface at 25 °C. The air-in-water system procedure followed the captive bubble technique, where the sample surface was immersed in water maintained at 25 °C and a small air bubble was placed on the sample surface from the bottom using a curved needle. The contact angle of each surface was measured on 10 spots, and the obtained values were averaged.

For dynamic contact angle measurements, the advancing (θ_{adv}) and receding (θ_{rec}) contact angles were obtained by extending and then contracting the volume (5.9 μL) of the water droplet using a motor-driven syringe at a rate of 1.88 μL/s for 3.1 s. The extending/contracting droplet was monitored with a CCD camera; each picture was captured every 67 ms, and 24 images were taken for both θ_{adv} and θ_{rec}, when the water droplet volume was changed at 1.88 μL/s. The contact angles were evaluated from video printouts of the droplet.

(14) Lee, J. H.; Kopeckova, P.; Kopecek, J.; Andrade, J. D. *Biomaterials* **1990**, *11*, 455.
(15) Desai, N. P.; Hubbell, J. A. *Macromolecules* **1992**, *25*, 226.
(16) Bergstrom, K.; Osterberg, E.; Holmberg, K.; Riggs, J. A.; Van Alstime, J. M.; Schuman, T. P.; Burns, N. L.; Harris, J. M. *Colloids Surf. A* **1993**, *77*, 159.
(17) Sofia, S. J.; Premnath, V.; Merrill, E. W. *Macromolecules* **1998**, *31*, 5059.
(18) Osterberg, E.; Bergstrom, K.; Holmberg, K.; Schuman, T. P.; Riggs, J. A.;. Burns, N. L; Van Alstine, J. M.; Harris, J. M. *J. Biomed. Mater. Res.* **1995**, *29*, 741.
(19) Mori, Y.; Nagaoka, S.; Takiuchi, H.; Kikuchi, T.; Noguchi, N.; Tanzawa, H.; Noishiki, Y. *Trans. Am. Soc. Artif. Internal Organs* **1982**, *28*, 459.
(20) Bergstrom, K.; Osterberg, E.; Holmberg, K.; Hoffman, A. S.; Schuman, T. P.; Kozlowski, A.; Harris, J. M. *J. Biomater. Sci. Polym. Ed.* **1994**, *6*, 123.
(21) Harris, J. M., Ed. *Poly(ethylene glycol) Chemistry. Biotechnical and Biomedical Applications*; Plenum Press: New York, 1992.
(22) Glass, J. E., Ed. *Hydrophilic Polymers, Performance with Environmental Acceptance*; American Chemical Society: Washington DC, 1996.
(23) Prime, K. L.; Whiteside, G. M. *J. Am. Chem. Soc.* **1993**, *115*, 10714.
(24) Gombotz, W. R.; Guanghui, W.; Horbett, T. A.; Hoffman, A. S. *J. Biomed. Mater. Res.* **1991**, *25*, 1547.
(25) Lee, J.; Martic, P. A.; Tan, J. S. *J. Colloid Interface Sci.* **1989**, *131*, 252.
(26) Jeon, S. I.; Andrade, J. D.; de Gennes, P. G. *J. Colloid Interface Sci.* **1991**, *142*, 159.
(27) Roosjen, A.; van der Mei, H. C.; Busscher, H. J.; Norde, W. *Langmuir* **2004**, *20*, 10949.
(28) Uchida, K.; Otsuka, H.; Kaneko, M.; Kataoka, K.; Nagasaki, Y. *Anal. Chem.* **2005**, *77*, 1075.
(29) Otsuka, H.; Nagasaki, Y.; Kataoka, K. *Biomacromolecules* **2000**, *1*, 39.

Protein Adsorption Study. A protein adsorption study, which is an important reference for cell attachment, was performed using SPR equipment. Before the protein adsorption study, three types of PEGylated surface were constructed on a gold sensor chip in the same manner as described above: PEG5k(3), PEG5k(1)/2k(3), and PEG5k(2)/2k(4). And then protein adsorption was estimated by flowing 100 μL of serum-containing medium (EBM-2 medium to culture HUVEC) at a flow rate of 10 μL/min at 37 °C under running PBS (pH 7.4, 0.15 M) on the three types of PEGylated surface and native gold surface. The magnitude of the SPR angle shift by this injection was measured from the data taken from the final part of the curve after the surfaces were rinsed, and assessed as the amount of protein adsorbed. As a control, protein adsorption on a bare gold surface was examined.

2. Cell Culture Study. *Construction of PEGylated Surface.* Glass slides were etched with a boiling mixture of 50% (v/v) sulfuric acid and 50% (v/v) hydrogen peroxide for 30 min and then rinsed thoroughly with water. At 10^{-6} Torr, a 10 Å film of chromium was vapor-deposited at a rate of 0.1 Å/s onto the glass substrate. A 200 Å film of gold was then vapor-deposited on top of it at a rate of 0.1 Å/s. PEGylated surfaces were prepared on the gold films in the same manner as described for SPR measurements. PBS (pH 7.4, 0.15 M, containing 1 M NaCl) solutions of PEG5k (0.01 mg/mL) and PEG2k (0.01 mg/mL) were prepared. Then, PEG solutions with the appropriate conditions were retained on the gold film for 30 min to construct the PEGylated surfaces described above (PEG5k(3), PEG5k(1)/2k(3), PEG5k(2)/2k(4)). The plates were washed with Milli-Q water between each PEGylation, for 5 min each time.

Micropatterning of PEGylated Surface. The micropattern on the PEGylated surfaces were obtained by $N_2 + H_2$ plasma etching using a metal mask with holes 100 μm in diameter spaced 300 μm apart. After construction of a 2-well plastic chamber (Falcon BD) on the glass thus prepared, all samples were sterilized with ethylene oxide gas.

Cell Culture Study. HUVECs were seeded onto the micropatterned PEGylated surface at a cell density of 1×10^6 cells/mL. Cells were cultured at 37 °C in a humidified atmosphere of 5% CO_2. An EBM-2 medium was used for cultivation and was exchanged every 2 days.

Results and Discussion

Micropatterned PEGylated substrates with two-dimensional arrays of plasma-etched circular domains (ϕ = 100 μm) were prepared by sequential immobilization of PEG possessing a mercapto group at the end of the chain on the gold substrate, followed by plasma etching through a metal mask pattern with circular holes. The PEGylated region on the patterned substrate acts to repel proteins and thus inhibits cell adhesion. Proteins are expected to adsorb from the serum-containing medium onto the plasma-etched circular domains, exposing the base gold surface.

1. PEG Immobilization Study. The surface properties of the PEG coating were studied in detail to estimate protein adsorption and subsequent cell culture study on PEGylated surfaces. First, PBS solutions of various concentrations of PEG including 1 M NaCl were injected onto the gold surface using an SPR instrument to optimize immobilized concentration on a sensor chip. Use of high ionic strength buffer caused an increase in the amount of immobilized PEG, due to the appreciably reduced solubility of PEG in concentrated buffer solution.[30] The changes in SPR angle at each concentration of PEG5k are plotted in Figure 1. The results confirmed that the amount of immobilized PEG increased with increases in the injected PEG concentration; saturation was observed at PEG concentrations over 0.01 mg/mL, suggesting that the amount of possible immobilization on the gold surface is constant with injection of PEG above this concentration. There were no significant differences in this PEG immobilization study between PEG2k and PEG5k. Therefore, immobilization of PEG

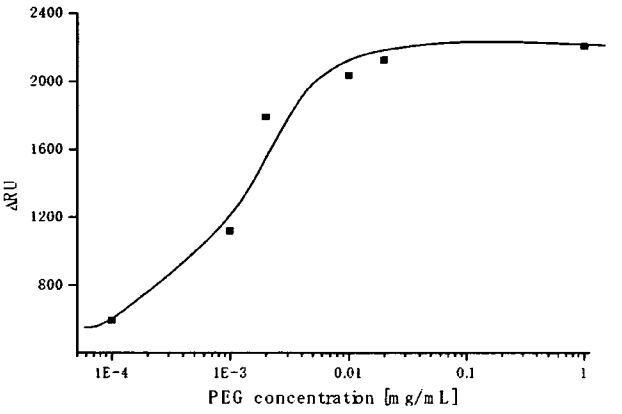

Figure 1. PEG immobilization as a function of PEG concentration. Flow rate, 10 μL/min; running buffer, PBS (pH 7.4, 0.15 M, containing 1 M NaCl); sample, PEG (M_w: 5k)/PBS (0.15 M, pH 7.4, containing 1 M NaCl) solution; sample injection, 100 μL.

on the gold surface was performed with 0.01 mg/mL PEG solution. Three types of PEG immobilization (PEG5k(3), PEG5k(1)/2k-(3), PEG5k(2)/2k(4), as described in the experimental section) were performed at this concentration, as shown in SPR sensorgrams (Figure 2). After first treatment with PEG5k, the sensor surface was washed under running buffer to remove noncovalently adsorbed PEG. The sensor chip was then treated again with a solution of PEG5k. This cycle of adsorption/rinsing of PEG5k was repeated several times. Eventually, the total SPR angle shift was amplified by increasing the number of treatment cycles to three, indicating that repetitive treatment with PEG5k was effective in increasing the density of PEG (PEG5k(3)). Notably, this trend became even more significant following additional treatment of the PEG5k surface with shorter PEG (PEG2k), as shown in Figure 2b,c. We planned to increase the surface brush density by PEG2k, retaining the PEG5k brush surface character. Sensorgrams showed a number of interesting findings. First, immobilization of long-chain PEG (PEG5k(1)) increased markedly with changes in SPR angle (Figure 2a–c). However, the extent of the shift decreased with the second injection of long-chain PEG (PEG5k(2)) (Figure 2a,c), and little change was seen on the third injection of long-chain PEG (PEG5k-(3)) (Figure 2a). On the other hand, immobilization of short-chain PEG (PEG2k(1)) after long-chain PEG resulted again in marked changes (Figure 2b,c). These results suggested that long-chain PEG5k can hardly penetrate into the preconstructed longer PEG-brushed layer due to its exclusion volume effect, while short-chain PEG2k appreciably filled the gap in the preconstructed longer PEG layer. It should be noted that SPR sensorgrams showed a steep increase curve in PEG2k(1), as shown in Figure 2b,c, indicating the importance of a short underbrushed PEG layer in increasing the PEG chain density.

To confirm that these SPR angle changes are reflected directly in the amount of immobilized PEG, QCM measurement was performed in the same manner as SPR (Table 1). The average value of total frequency shift after PEG injection is given as Δf in Table 1. PEG5k(2)/2k(4) surface showed the largest frequency shift, and PEG5k(1)/2k(3) surface also showed around 2000 Hz in frequency shift. On the other hand, PEG5k(3) surface showed around 1400 Hz in total frequency shift. Thus, PEG5k surface mixed with PEG2k showed larger mass change than only PEG5k chain immobilization, which suggested that more PEG chains were immobilized in PEG5k and PEG2k mixed surface. This result also indicated a significant role of a short underbrushed PEG layer in increasing the PEG chain density. On QCM

(30) Emoto, K.; Harris, J. M.; Alstine, M. V. *Anal. Chem.* **1996**, *68*, 3751.

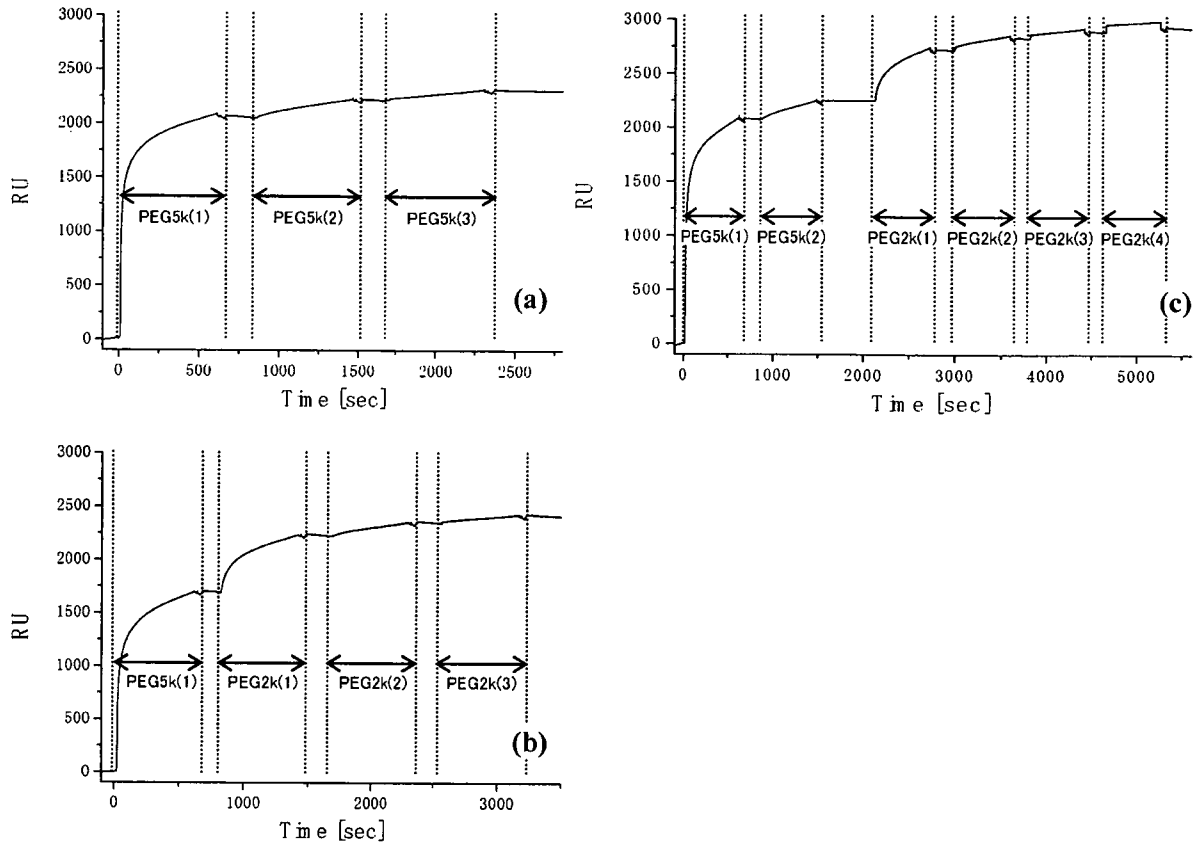

Figure 2. Sensorgrams of PEG immobilization on gold surfaces. (a) PEG5k(3), (b) PEG5k(1)/2k(3), and (c)PEG5k(2)/2k(4). Flow rate, 10 μL/min; running buffer, PBS (0.15 M, pH 7.4, containing 1 M NaCl); sample, 0.01 mg/mL of PEG (M_w: 5k or 2k)/PBS (0.15 M, pH7.4, containing 1 M NaCl) solution; sample injection, 100 μL for each time point.

Table 1. Comparison of Three Types of PEG Immobilization Measured by QCM: Δf is the Average of Total Frequency Shift after PEG Immobilization (n = 3)

PEG surfaces	Δf(Hz)	±S.D.
5k(3)	1382.8	118.6
5k(1)/2k(3)	1922.8	92.70
5k(2)/2k(4)	2144.7	81.74

measurement, the PEG5k(2)/2k(4) surface was determined to have the highest PEG chain density, while PEG5k(3) had the lowest.

The static wettability of the surface coated with PEG was estimated in both air and water by contact angle measurement (Figure 3). In the water-in-air measurement, the coating of PEG on the gold substrate significantly increased its wettability, as indicated by a decrease in the static contact angle (~30°). A similar trend was observed in the air-in-water measurement and the effect of PEG density on wettability was more pronounced, showing progressively increasing contact angle with increasing PEG chain density. Note that the increase in contact angle corresponds to an increase in wettability for the air-in-water system. As the accuracy of contact angle is ±2°, as shown by Zisman and co-worker,[31] significant differences could be seen between PEG surfaces. Furthermore, advancing/receding contact angles and hysteresis were measured on each PEG surface to estimate the dynamics of the uppermost surface in detail (Figure 4). In receding contact angles, each PEG surface showed a small value of around 15−20° and there was little difference between surfaces. On the other hand, critical differences were observed

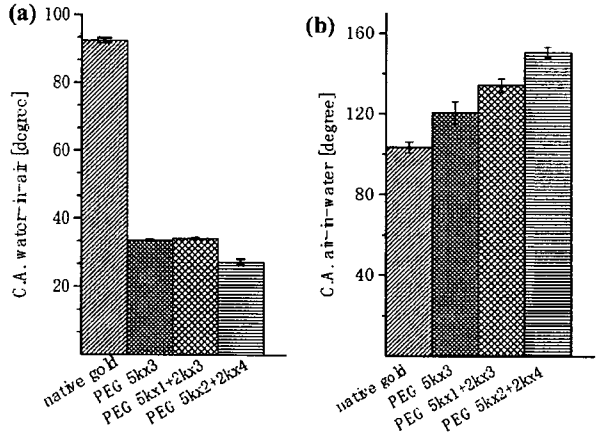

Figure 3. Static water contact angles on PEGylated gold surface. (a) Water-in-air system; (b) air-in-water system.

in advancing contact angles. PEG5k(3) and PEG5k(1)/2k(3) surfaces had around 30°, while the value for the PEG5k(2)/2k(4) surface was almost half. As PEG surfaces are easy to hydrate and show good water retentivity, once they became wet, receding contact angles showed small values in all PEG surfaces, resulting in little difference in receding contact angle. In contrast, significant differences were observed in advancing contact angles, indicating that the PEG5k(2)/2k(4) surface has the greatest wettability in the dry to wet state as compared with the other PEG surfaces examined. Hysteresis indicated differences between PEG5k(2)/2k(4) surfaces and the other surfaces according to its high surface free energy. When the water droplet extends, the surface with

(31) Fox, H. W.; Zisman, W. A. *J. Colloid Sci.* **1950**, *5*, 514.

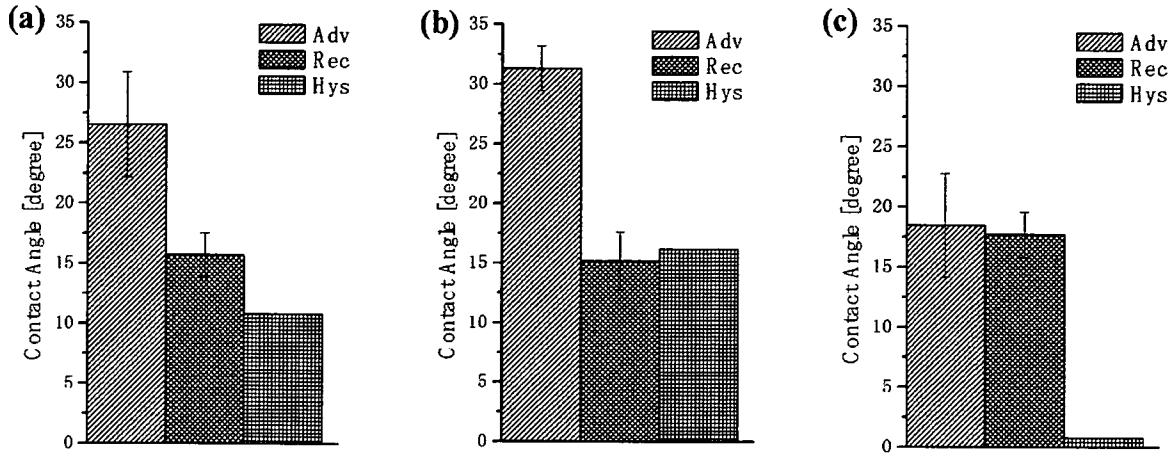

Figure 4. Dynamic water contact angles on PEGylated gold surfaces. (a) PEG5k(3), (b) PEG5k(1)/2k(3), and (c) PEG5k(2)2k(4).

a high surface free energy facilitates penetration of water, aiding in water droplet spreading, while the surface prevents the water droplet from receding when it contracts. Accordingly, the observations of the present study suggested that the PEG5k-(2)/2k(4) surface is the most hydrophilic and has a high surface free energy due to its high PEG chain density. Furthermore, the chain density is reported to have the relation with other parameters including the thickness and conformation of PEG layer.[23−27,32,33] The PEG chains (5k and 2k) are more well-oriented in this surface since the short, filler-like PEG2k chains will enhance the lateral interactions (e.g., hydrogen bonding and van der Waals force) between the PEG chains. This will likely result in much enhanced water affinity/penetration capability in PEG chains during the advancing angle measurement. Therefore, only small hysteresis value will be found on a PEG5k(2)/2k(4) surface.

Nonspecific protein adsorption from the culture medium for HUVEC was estimated on each PEG-coated surface to estimate the cytophobicity of PEGylated surfaces because the adsorbed proteins are responsible for subsequent cell adhesion. On bare gold as a control, the SPR angle shift due to the nonspecific adsorption of protein was 2927.4 RU, when a serum-containing cell (HUVEC) culture medium (EBM-2) was passed over the surface for 10 min at a flow rate of 10 μL/min. In contrast, PEG-coated surfaces clearly reduced protein adsorption (Figure 5). Figure 5 also shows a comparison of protein adsorption on the three types of PEG surface. The SPR angle shift was 676.5, 350.8, and 218.0 RU on PEG5k(3), PEG5k(1)/2k(3), and PEG 5k(2)/2k(4) surfaces, respectively. The PEG5k(2)/2k(4) surface showed the greatest degree of inhibition of protein adsorption from the medium, suggesting that the inhibitory effect of nonspecific protein adsorption was the highest for this surface among those studied. The physicochemical properties of PEG surfaces described above indicate that PEG surfaces with higher immobilized PEG chain density have greater ability to repel proteins. Based on these results, it was concluded that shorter PEG, viz. an underbrushed layer to increase the PEG surface density, played a substantial role in minimizing nonspecific protein adsorption. Other workers have also proposed that PEG mixtures, which are polydisperse with respect to molecular weight, are more efficacious than single molecular weights. Mixed PEGs were shown to have greatest efficacy in steric stabilization of colloidal particles and in protein repellency.[34,35] The PEG5k-

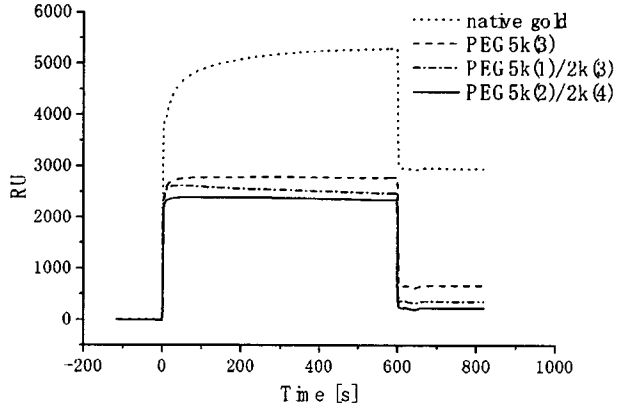

Figure 5. Sensorgrams of injection of serum-containing cell culture medium (EBM-2 medium to culture HUVEC) on native gold and each PEGylated surfaces. Flow rate, 10 μL/min; running buffer, PBS (pH 7.4, 0.15 M); sample injection volume, 100 μL.

(2)/2k(4) surface with the highest PEG chain density was expected to have the highest cytophobicity.

2. Cell Culture Study. Gold surfaces were coated with PEG to inhibit nonspecific protein adsorption and were expected to act as cytophobic surfaces for subsequent cell patterning. The PEG-coated gold substrates were micropatterned by plasma etching ($N_2 + H_2$) through a metal mask pattern with ϕ100 μm circular holes separated by 300 μm (edge-to-edge distance), and cell culture dishes were then set onto these surfaces (2 × 2 cm). Microscopic images following seeding of HUVEC on the surfaces are shown in Figure 6. On PEG5k(3) surfaces with lower PEG chain density as suggested by physicochemical studies, seeded HUVEC showed disorganized cellular attachment regardless of micropatterned substrate (Figure 6a). On the other hand, the PEG5k(1)/2k(3) surface (Figure 6b) and PEG5k(2)/2k(4) surface (Figure 6c) showed patterned cell attachment due to the suggested higher PEG chain density compared with that of the PEG5k(3) surface, although cells that had overgrown beyond the pattern were still observed on PEG5k(1)/2k(3) surfaces. The results of cultivation of HUVECs for 1 week are shown in Figure 6d−f. Arrayed cellular attachment was observed only on the PEG5k-(2)/2k(4) surface (Figure 6f). In contrast, the HUVECs began to bridge across multiple islands on the PEG5k(1)/2k(3) surface (Figure 6e) and this bridging was more pronounced to form a complete cell sheet on the PEG5k(3) surface (Figure 6d). It is

(32) Harder, P.; Grunze, M.; Dahint, R.; Whitesides, G. M.; Laibinis, P. E. *J. Phys. Chem.* **1998**, *102*, 426.
(33) Zhu, B.; Eurell, T.; Gunawan, R.; Leckband, D. *J. Biomed. Mater. Res.* **2001**, *56*, 406.
(34) Stenkamp, V. S.; Berg, J. C. *Langmuir* **1997**, *13*, 3827.
(35) Pavey, K. D.; Olliff, C. J. *Biomaterials* **1999**, *20*, 885.

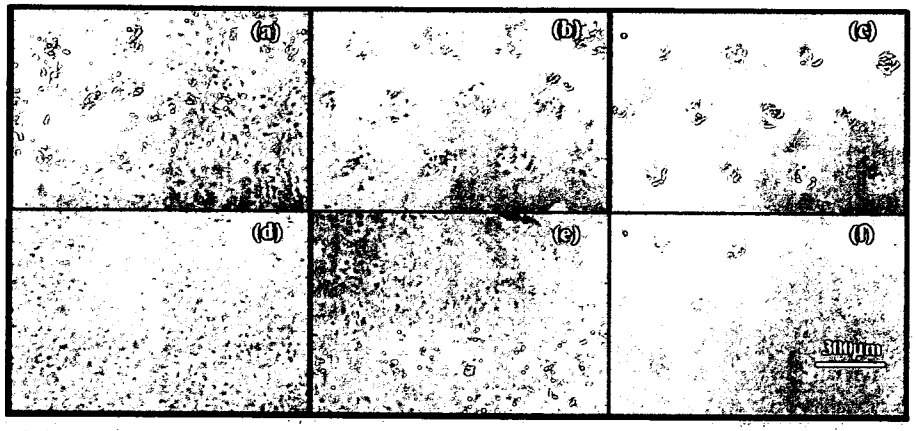

Figure 6. Microscopic image of cell seeding study. After 1 day of culture of HUVEC on micropatterned (a) PEG5k(3) surface, (b) PEG5k(1)/2k(3) surface, and (c) PEG5k(2)/2k(4) surface. After 1 week of culture of HUVEC on micropatterned (d) PEG5k(3) surface, (e) PEG5k(1)/2k(3) surface, and (f) PEG5k(2)/2k(4) surface.

clear that PEG chain density affects pattern recognition in cell attachment. The threshold density for HUVEC bridging seems to exist on the surface between PEG5k(3) and PEG5k(2)/2k(4). Cells overgrew beyond the pattern on weak protein-repellent surfaces. In addition, when overgrown cells grew sufficiently close together, bridging occurred between overgrown cellular patterns. Attached patterns eventually resulted in sheet formation. As described above, no pattern recognition of cell attachment was seen on the surfaces coated only with long-chain PEG (PEG5k(3)) because of its lower inhibitory effect on nonspecific protein adsorption. In contrast, cell array formation was observed by constructing long- and short-chain PEG mixed surfaces. Furthermore, PEG5k(2)/2k(4) surfaces showed the least nonspecific cell attachment in contrast to some nonspecific cell attachment and bridging of cellular islands on PEG5k(1)/2k(3) surfaces. SPR results indicated that cell-adhesive proteins are greatly repelled on PEG5k(2)/2k(4) surfaces to promote pattern recognition of cell attachment. Some cell attachment between cellular islands was confirmed on PEG5k(3) and 5k(1)/2k(3) surfaces after 1 day in culture, and the attached cells extended toward each other and bridging occurred across cellular islands. Bridged cellular patterns grew everywhere on the surface and eventually formed a complete cell sheet. As the first cell attachment on the cytophobic region depends on the ability of the surface to repel protein, surfaces with lower PEG chain density (PEG5k(3) or PEG5k(1)/2k(3)) resulted in cell attachment and cell sheet formation. Thus, the results of the cell culture study agreed well with the surface properties, suggesting that PEG chain density played a critical role in micropatterned cell attachment.

Conclusions

To gain insight into the design of cellular microenvironments, we examined the micropatterning of endothelial cells on microfabricated gold substrates coated with PEG brushes in terms of the relationship between PEG chain density and cellular attachment. A PEG-brushed layer was constructed on a gold substrate using PEG with a mercapto group at the chain end. After treatment with longer chain PEG with a molecular weight of 5000, shorter chain PEG (2000) was introduced onto the gold substrate to modulate the chain density. In this way, PEGylated surfaces with different chain densities were produced, and subsequent micropatterning was achieved by plasma etching through a micropatterned metal mask. The results indicated that cell pattern formation was strongly dependent on both the PEG chain density and the extent of protein adsorption, as evidenced by physicochemical and biological characterization of PEGylated surfaces using SPR, QCM, and static/dynamic contact angle measurements. Cell micropatterning showed long-term retention only on the surfaces with greater disparity between cytophobic and cytophilic regions. Notably, a PEG chain density sufficiently high to inhibit outgrowth of endothelial cells beyond the cytophilic gold region to the cytophobic PEGylated region could be obtained only on the mixed PEG chain-tethered surface, which achieved almost complete prevention of nonspecific protein adsorption. These observations clearly indicated that shorter PEG, viz. an underbrushed PEG layer to increase the PEG surface density, played a substantial role in minimizing nonspecific protein adsorption and long-term maintenance of the active cell pattern. It should be noted that the precise control of surface properties in single-molecule order directly affected micropatterned cellular attachment. Therefore, we envision the cellular micropatterning technique presented here becoming a valuable tool for the control of cell−surface and cell−cell interactions on a micrometer scale and to evaluate local effects of engineered microenvironments on cellular behavior. The surface fabrication technique studied here is a promising technology for the development of tissue/cell-based biosensors and in the field of tissue engineering.

Acknowledgment. Microfabrication using the plasma etching technique was conducted at the National Institute for Materials Science (NIMS), Japan, with assistance from Dr. Y. Horiike. Financial support for this work was partly provided by Special Coordination Funds for Promoting Science and Technology and also supported by Research Promotion Bureau under contract nos. 15-99 and 15-396, both from the Ministry of Education, Culture, Sports, Science, and Technology (MEXT), Japan. Part of this work was also supported financially by a Grant-in-Aid for Research on Health Sciences for Drug Innovation (KH71066), Ministry of Health, Labor, and Welfare of Japan, and The New Energy and Industrial Technology Development Organization (NEDO).

LA0624384